

Image segmentation based on the hybrid total variation model and the K-means clustering strategy

Baoli Shi[†], Zhi-Feng Pang[†] and Jing Xu[§]

[†]*College of Mathematics and Statistic, Henan University, kaifeng, 475004, China.*

[§]*School of Statistic and Mathematics Zhejiang Gongshang University, Hangzhou, 310012, China*

Abstract The performance of image segmentation highly relies on the original inputting image. When the image is contaminated by some noises or blurs, we can not obtain the efficient segmentation result by using direct segmentation methods. In order to efficiently segment the contaminated image, this paper proposes a two step method based on the hybrid total variation model with a box constraint and the K-means clustering method. In the first step, the hybrid model is based on the weighted convex combination between the total variation functional and the high-order total variation as the regularization term to obtain the original clustering data. In order to deal with non-smooth regularization term, we solve this model by employing the alternating split Bregman method. Then, in the second step, the segmentation can be obtained by thresholding this clustering data into different phases, where the thresholds can be given by using the K-means clustering method. Numerical comparisons show that our proposed model can provide more efficient segmentation results dealing with the noise image and blurring image.

Keywords: Potts Model, Alternating Direction Method of Multipliers(ADMM), Primal-dual Method(PDM), Data Clustering

1 Introduction

Image segmentation has become increasingly important in the last decade, due to a fast expanding field of applications in image analysis and computer vision. It aims to separate objects of interest from each others or from the backward or find boundaries of such objects. Until now, a wide variety of techniques including variational partial differential equation (PDE) image segmentation methods [10, 20, 32, 12, 14], histogram analysis, region growing and edge detection [49, 39] have been proposed to solve the image segmentation problem.

The variational segmentation methods are characterized by deriving an energy functional from some a priori mathematical model and minimizing this energy functional over all possible partitions. Among them, the region-based models [12, 14] have been proposed and applied to the image segmentation field by incorporating region information so that image within each segmented region has a uniform characteristic such as intensity and texture. The most well-known region-based model is the Mumford and Shah (MS) model [32], in which an image is decomposed into a set of regions within the bounded open set and these regions are separated by smooth edges.

[†]This work is supported by NSF of China (Nos.U1304610,11001239,11101365, 11401170,11426137), Foundation of Henan Educational Committee of China (Nos.14A110018, 14B110019) and the National Basic Research Program of China (973 Program)(No.2015CB856003..

E-mail address:baolishi1983@163.com; zhifengpang@163.com; jingxu@amss.ac.cn

The difficulty in studying the MS model is that it involves two unknowns: the intensity function and the set of edges. So the MS model is hard to implement in practice since the discretization of the unknown set of edges is a very complex task. In order to effectively solve the MS model, Chan and Vese (CV) [14] proposed an easily handle model by assuming that the segmentation result was a piecewise constant image with two different constant values. The CV model has achieved good performance in image segmentation task because of its ability to obtain a larger convergence range and handle topological changes naturally [41]. However, more work needs to be done on effective representation of regions and their boundaries for multi-phase segmentation. Vese and Chan extended the work in [40] to utilize multi-phase level set functionals to represent multiple regions. Similar to the two-phase case, the model is non-convex and thus the global minimization can not be guaranteed. In order to overcome these drawbacks, convex relaxation methods [12, 4, 5] and graph cut [6, 2, 16, 19, 21, 48] method were proposed in this field.

During some phases of obtaining a real image, we can only get a contaminated image due to the interference of some random noises and blurs. This interference leads not to obtain an expected segmentation results by using classical methods such as the MS model and clustering methods. So it is very important to suppress these contaminated information before segmenting the image [21, 18, 35, 33]. Recently a two step method based on the MS model was proposed in [8]. The first step is through restoring the contaminated image to obtain a smooth solution by using the modified MS model under the space $W^{1,2}(\Omega)$ for the image domain $\Omega \subset R^2$. Once the restored image is obtained, the second stage is to threshold it into different phases by using the K-means clustering method. However, the image space is not continuous in the region of edges, so the space $W^{1,2}(\Omega)$ used in [8] is not suitable. Moreover, the image pixel value represents physical quantity such as photon count or energy, which is often non-negative and has a upper bound or saturated value due to the finite number of bits being used for image representation. An intuitive approach is to solve the unconstrained problem and then project the restored values in the original chosen range. However, this approach results in the presence of spurious ripples in the restored image. Chopping off these projection values may also introduce patches of black color which could be visually unpleasant. Therefore, imposing a priori constraint is a natural requirement for the image restoration problem. In this paper, by generalizing above two-step strategy to a more suitable space, we propose a two-step method for the image segmentation problem. The motivation of our work is to present a hybrid total-variation model in the first step by combining edge based method with region based method to improve the efficiency of traditional models in [26, 36, 25]. Furthermore, we constrain pixel values in this step to lie in a certain dynamic range in order to improve the preconditioning results. In addition, the proposed model is solved by an algorithm based on the alternating split Bregman method, which can guarantee the implementation efficiency with respect to the resultant image quality based on the convergence of this method. Once the solution is obtained, we set it as the inputting data in the second step and use the K-means clustering method to threshold it into expected phases. Then we can obtain the segmentation by setting related regions to be different constants in these phases. The numerical experiments show that our proposed model and method are very effective for segmenting the degraded image.

The rest of the paper is organized as follows. In Section 2, we review some works in the image segmentation problem under the energy minimization framework. In section 3, we propose the hybrid total variation model with a constraint and then employ the split Bregman method to solve it as the first step. In the second step, we give the detail of how to threshold the clustering data generated by the K-means clustering method into different phases. In Section 4, we present some experimental results of our proposed strategy and compare their performance with the reviewed models in Section 2. Some conclusions are drawn in Section 5.

2 Related works

Before we go into the details of our proposed hybrid total-variation segmentation models, we first review some works that are closely related to this paper.

2.1 Mumford-Shah (MS) model

The MS model is an established image segmentation model with a wide range of applications. An energy functional to be minimized is to find the set of discontinuities Γ or the edge set, and a piecewise smooth approximation u of a given image intensity function $f : \Omega \subset \mathbb{R}^2 \rightarrow \mathbb{R}$. Formally, the MS model can be written as

$$\min_{u, \Gamma} \left\{ \frac{1}{2} \|f - u\|_{L^2(\Omega)}^2 + \lambda \int_{\Omega \setminus \Gamma} |\nabla u|^2 dx + \gamma \text{Length}(\Gamma) \right\}, \quad (2.1)$$

where λ and γ are positive constants. However, the problem is hard in this form, as the two variables u and Γ of the optimization are of very difficult natures; the edge set Γ may be quite general and may exhibit singularities. As alternative solutions to this problem, many works have been done to simplify or modify the general MS model (2.1).

2.2 The piecewise constant (PC) model

The piecewise constant Mumford-Shah model is a simpler model obtained by assuming that image approximation is constant inside each connected component (i.e. $u = c_i$, where c_i is a constant). At this point, the MS model can be simplistically rewritten as

$$\min_{c_i, \Gamma} \sum_{i=1}^{\mathcal{M}} \int_{\Omega_i} |f - c_i|^2 dx + \gamma \text{Length}(\Gamma) \quad (2.2)$$

such that $\bigcup_{i=1}^{\mathcal{M}} \Omega_i = \Omega \setminus \Gamma$ and $\Omega_i \cap \Omega_j = \emptyset$ if $i \neq j$, where \mathcal{M} is the number of connected components.

To minimize the model (2.2), the zero level set $\Gamma =: \{x \in \Omega | \phi(x) := 0\}$ is used to replace the unknown curve Γ_i , where $\bigcup_{i=1}^{\mathcal{M}} \Gamma_i = \Gamma$. For the case $\mathcal{M} = 2$, the model (2.2) is the classical CV model [14], where Chan and Vese proposed to alternately obtain the curve Γ and the constant values c_1 and c_2 by solving the following variational formulation

$$\begin{cases} c_1(\phi) = \frac{\int_{\Omega} f H(\phi) dx}{\int_{\Omega} H(\phi) dx}, \\ c_2(\phi) = \frac{\int_{\Omega} f (1-H(\phi)) dx}{\int_{\Omega} (1-H(\phi)) dx}, \\ \frac{\partial \phi}{\partial t} = \delta(\phi) \left[\gamma \operatorname{div} \frac{\nabla \phi}{|\nabla \phi|} - (f - c_1)^2 + (f - c_2)^2 \right], \end{cases} \quad (2.3)$$

where $H(\cdot)$ is the Heaviside function. Different from the CV model, the problem for $\mathcal{M} > 2$ is more challenging. The main difficulty is to find effective representations of regions and their boundaries. Several recent works are related to this problem. Vese and Chan [40] proposed to use the four color theorem to provide segmentation for any number of objects in Ω . One level set function can only separate two classes, hence $m_1 = \log_2 \mathcal{M}$ is the number of level sets necessary to segment \mathcal{M} distinct classes. A variant of the level set method in [27], the so-called

piecewise constant level method (PCLSM), expresses the energy in terms of a labeling function. They proposed to use binary level set functions which took value 1 and -1 instead of using the classical continuous level set function as did in [40, 14]. Unfortunately, the main disadvantage of both level set methods is their probable of getting stuck in a possibly inferior local minima because of their nonconvex formulations.

2.3 The Potts model

In the work of [12], Chan et al obtained global optimal solution of the CV model when the two piecewise constant values are first known. The key idea is to relax the characteristic function in such a way that the characteristic function minimizers can be obtained from the minimizers of the relaxed problem by a simple thresholding procedure. This allows the non-convex Chan-Vese problem to be globally solved by using standard convex minimization methods. Following this work and the assumption that we know the values of every piecewise constant, the multiphase segmentation problem (2.1) can be written as

$$\min_{\Gamma} \sum_{i=1}^{\mathcal{M}} \int_{\Omega_i} |f - c_i|^2 dx + \gamma \text{Length}(\Gamma). \quad (2.4)$$

Actually, in this case, each pixel is assigned one of region labels (i.e. the known piecewise constants). Assume that a labeling $l : \Omega \rightarrow \{c_1, c_2, \dots, c_{\mathcal{M}}\}$ indicates the m regions each pixel belongs to $\Omega_i = \{l(x) = c_i\}$, we introduce the indicator function $u := (u_1, u_2, \dots, u_{\mathcal{M}}) \in BV(\Omega, \{0, 1\})^{\mathcal{M}}$

$$u_i(x) = \begin{cases} 1 & \text{if } l(x) = c_i \\ 0 & \text{otherwise} \end{cases}$$

for $i = 1, 2, \dots, \mathcal{M}$, where BV refers to the bounded variation space, then the model (2.4) can be reduced to the formulation of the Potts model

$$\min_{u \in \mathcal{C}_1} \sum_{i=1}^{\mathcal{M}} \left\{ \int_{\Omega} |f - c_i|^2 u_i dx + \gamma \int_{\Omega} |\nabla u_i| dx \right\}, \quad (2.5)$$

where $\mathcal{C}_1 := \left\{ u \in \{0, 1\}^{\mathcal{M}} \mid \sum_{i=1}^{\mathcal{M}} u_i = 1 \right\}$.

The above Potts model is a nonconvex problem due to the binary constraints. A major class of methods is based on the convex relaxation of the admissible set by allowing for the labeling functions to take intermediate values from the unit simplex. That is to say, the problem (2.5) is transformed into

$$\min_{u \in \mathcal{C}} \sum_{i=1}^{\mathcal{M}} \left\{ \int_{\Omega} |f - c_i|^2 u_i dx + \gamma \int_{\Omega} |\nabla u_i| dx \right\}, \quad (2.6)$$

where $\mathcal{C} := \left\{ u \in [0, 1]^{\mathcal{M}} \mid \sum_{i=1}^{\mathcal{M}} u_i = 1 \right\}$. Then we can solve this relaxed version by using some operator splitting methods [22, 23, 47]. If the minimizer of the problem (2.6) happens to be binary everywhere, it is also a global minimizer of the original problem (2.5). However, unlike the two label problem [14], if the computed minimizer of the problem (2.6) is not binary, there is no thresholding scheme which can keep a binary global minimizer of (2.5). Even if such a binary

minimizer exists, the problem (2.6) may result in nonbinary solutions due to non-uniqueness. Then a approximated strategy is to use the indicator function of the largest component u_i as an approximate binary solution [22, 23, 47]. Graph-based optimization techniques have been used as components in optimization methods for functionals formulated in the continuous space. Boykov and Cremers [6] proposed to use a max-flow/min-cut step to assist in level set updates. Grady [19] employed a max-flow/min-cut operation as a component of their piecewise constant Mumford-Shah complete computations. More recently, Bae etc. proposed a smooth dual model of the Potts model in [1]. Pock etc. [35] developed a tight convex relaxation framework for Potts model. Yuan etc [44, 45] have designed a max-flow approach to the Potts model.

2.4 The convex variant of the MS model

Based on the observation about binary images: a binary image can be recovered quite well from its smoothed version by thresholding with a proper threshold, Cai et al [8] recently proposed to use two stages for the image segmentation problem. In their scheme, the first stage is to find a smooth image g that can facilitate the segmentation, and then the second stage is to threshold g to reveal different segmentation features by using one of chosen thresholds based on the K-means clustering method. Specially, this course can be formulated as

- The first step is to compute g by

$$\min_g \|f - \mathcal{A}g\|_{L^2(\Omega)}^2 + \lambda \int_{\Omega} |\nabla g|^2 dx + \gamma \int_{\Omega} |\nabla g| dx, \quad (2.7)$$

where f denotes the degraded image modeled by $f = \mathcal{A}g + \eta$ and \mathcal{A} is a suitable linear operator. Here η denotes some noises.

- The second step is to obtain the segmentation by segmenting g using properly chosen thresholds, which is generated by the K-means clustering method.

Actually, they used the fact that $\int_{\Gamma} |\nabla g|^2 dx = 0$ when $g \in W^{1,2}(\Omega)$, then the problem (2.7) is equivalent to the original MS model (2.1). Note that here $W^{a,b}(\Omega)$ denotes the Sobolev space defined by $W^{a,b}(\Omega) := \left\{ u : u \in L^b(\Omega), D^\alpha u \in L^b(\Omega) \ 0 \leq |\alpha| \leq a \right\}$, where $D^\alpha := D_1^{\alpha_1} D_2^{\alpha_2} \cdots D_r^{\alpha_r}$ with $\sum_{i=1}^r \alpha_i = |\alpha|$ and $D_j = \frac{\partial}{\partial x_j}$. The problem (2.7) is a non-smooth optimization problem, so they employed the splitting Bregman method to solve it.

3 The segmentation model based on constrained hybrid total variation model

In this section, we will introduce our proposed model following from the problem (2.7) and bring out its salient merits and numerical method. In the problem (2.7), there include a fitting term and two regularization terms. Its nature is the image restoration problem, so the segmentation result extremely depends on the restored image. However, the global parameters λ and γ can not depict the local properties while the image owns complex structures. Furthermore, image values which represent physical quantities such as photon counts or energies are often non-negative and also have the upper bound or saturated value, so it is a natural requirement to impose a priori constraint on the proposed model.

3.1 The proposed model of the first step

The total variation type models have been extensively used in image restoration such as the ROF model [36] and the higher-order model [3, 13, 28, 46]. However, these two classes of models respectively keep image edges or only keep image smoothing regions. On the other hand, image value represents physical quantities such as photon counts or energies, which is often non-negative and also has the upper bound or saturated value due to finite number of bits being used for image representation. This is particularly true in applications such as astronomical image [29, 38]. Therefore, imposing a priori constraint is a natural requirement for the deblurring problem. To effectively overcome these drawbacks, some hybrid models based on the total variation functional have been noticed. Following the problem (2.7), we propose the following variational problem

$$\min_{g \in [0, t]} \|f - \mathcal{A}g\|_{L^2(\Omega)}^2 + \lambda \int_{\Omega} (1 - \omega(x)) |\nabla^2 g| dx + \gamma \int_{\Omega} \omega(x) |\nabla g| dx, \quad (3.8)$$

where $\omega(x) \in (0, 1)$ is a weighted function related to the region structures of the inputting image. Obviously, we replace the second term in the problem (2.7) by $\int_{\Omega} |\nabla^2 g| dx$, which actually requires $u \in W^{2,1}(\Omega)$, then we can obtain more efficient restored image. However, this space have not a reflexive solution of the minimization problem by the direct calculus of the problem (3.8). Actually, we can extend it to a larger space as being done in [25, 34]. Furthermore, we also add the weighted function $\omega(x)$ with formally convex combination of $\int_{\Omega} |\nabla^2 g| dx$ and $\int_{\Omega} |\nabla g| dx$. This paper chooses the weighed function to be the edge indicator function. Thus edges can be found and retained during restoration process in the first stage of our proposed method.

Definition 3.1. $BV^{\kappa}(\Omega)$ is a subspace of functions $u \in L^1(\Omega)$ such that the following quantity is satisfied:

$$\int_{\Omega} |\mathbb{D}^{\kappa} u| = \sup \left\{ \int_{\Omega} u \operatorname{div}^{\kappa} p dx \mid p \in C_c^{\kappa}(\Omega, R^{2 \times \kappa}), \|p\|_{L^{\infty}} \leq 1 \right\} < \infty,$$

where

$$\|p(x)\|_{\infty} = \left\| \sqrt{\sum_{j=1}^2 \sum_{i=1}^{\kappa} (p^{i,j})^2} \right\|_{L^{\infty}}$$

for $\kappa = 1, 2$. Here $C_c^{\kappa}(\Omega)$ denotes the space of continuously differentiable vector-valued functions on Ω with compact support.

It is obviously that $BV(\Omega)$ and $BV^2(\Omega)$ are a Banach space respectively equipped with norms $\|u\|_{BV(\Omega)} = \|u\|_{L^1(\Omega)} + |\mathbb{D}u|(\Omega)$ and $\|u\|_{BV^2(\Omega)} = \|u\|_{BV(\Omega)} + |\mathbb{D}^2 u|(\Omega)$ [25, 34].

Theorem 3.1. Let Ω be a bounded connected open subset of R^2 with the Lipschitz boundary. Assume that $f \in BV(\Omega) \cap BV^2(\Omega) \cap L^{\infty}(\Omega)$. Then the problem

$$\min_{g \in [0, t]} \|f - \mathcal{A}g\|_{L^2(\Omega)}^2 + \lambda \int_{\Omega} (1 - \omega(x)) |\mathbb{D}^2 g| + \gamma \int_{\Omega} \omega(x) |\mathbb{D}g|, \quad (3.9)$$

has a minimizer $g^* \in BV(\Omega) \cap BV^2(\Omega) \cap L^{\infty}(\Omega)$.

Proof. By introducing an indicator function

$$\delta_{\mathcal{D}}(g) = \begin{cases} 0, & \text{if } g \in \mathcal{D}, \\ \infty, & \text{if } g \notin \mathcal{D} \end{cases} \quad (3.10)$$

with $\mathcal{D} := [0, \iota]$, then we can write the problem (3.9) as

$$\min_g \|f - \mathcal{A}g\|_{L^2(\Omega)}^2 + \lambda \int_{\Omega} (1 - \omega(x)) |D^2 g| + \gamma \int_{\Omega} \omega(x) |Dg| + \delta_{\mathcal{D}}(g). \quad (3.11)$$

Then the problem (3.11) is the strictly convexity. So based on the work in [25], we can use the similar method to obtain above results. \square

3.2 The split Bregman method to solve the problem (3.8)

In this subsection we work with the discretized version of the problem (3.15) and assume a periodic boundary condition for g . By choosing the periodic boundary condition, the action of each of discrete differential operators can be regarded as a circular convolution of the image g and allows the use of fast Fourier transform (FFT). For a vector field $\boldsymbol{\nu} : R^{s \times t} \rightarrow R^{\tau}$, we respectively define the discretization norm $|\cdot|_1$ and $\|\cdot\|_2$ corresponding to the norms ℓ^1 and ℓ^2 with $\boldsymbol{\nu} = (\nu^1, \nu^2, \dots, \nu^{\tau})$ as follows

$$|\boldsymbol{\nu}|_1 = \sum_{i=1}^s \left(\sum_{j=1}^t (\nu_{i,j})^2 \right)^{\frac{1}{2}} \quad \text{and} \quad \|\boldsymbol{\nu}\|_2 = \left(\sum_{i=1}^s \sum_{j=1}^t (\nu_{i,j})^2 \right)^{\frac{1}{2}}.$$

In the following, we define the discrete gradient $\nabla u_{i,j} = (D_x^+ u_{i,j}, D_y^+ u_{i,j})$ as a forward difference operator

$$D_x^+ u_{i,j} = \begin{cases} u_{i+1,j} - u_{i,j} & \text{if } 1 \leq i < m, 1 \leq j \leq n \\ u_{1,j} - u_{i,j} & \text{if } i = m, 1 \leq j \leq n, \end{cases}$$

$$D_y^+ u_{i,j} = \begin{cases} u_{i,j+1} - u_{i,j} & \text{if } 1 \leq i \leq m, 1 \leq j < n \\ u_{i,1} - u_{i,j} & \text{if } 1 \leq i \leq m, j = n. \end{cases}$$

Similarly, we can also define the backward difference operator as

$$D_x^- u_{i,j} = \begin{cases} u_{i,j} - u_{i-1,j} & \text{if } 1 < i \leq m, 1 \leq j \leq n \\ u_{i,j} - u_{m,j} & \text{if } i = 1, 1 \leq j \leq n, \end{cases}$$

$$D_y^- u_{i,j} = \begin{cases} u_{i,j} - u_{i,j-1} & \text{if } 1 \leq i \leq m, 1 < j \leq n \\ u_{i,j} - u_{i,n} & \text{if } 1 \leq i \leq m, j = 1. \end{cases}$$

Then we can obtain

$$\nabla^2 u_{i,j} = (D_x^-(D_x^+ u_{i,j}), D_x^-(D_y^+ u_{i,j}), D_y^+(D_x^- u_{i,j}), D_y^+(D_y^- u_{i,j})).$$

Using the divergence theorem

$$-\text{div} \boldsymbol{\rho} \cdot u = \boldsymbol{\rho} \cdot \nabla u \quad \text{and} \quad \text{div}^2 \mathbf{p} \cdot u = \mathbf{p} \cdot \nabla^2 u$$

for $\forall u \in R^{m \times n}$, $\boldsymbol{\rho} \in R^{m \times n} \times R^{m \times n}$, $\mathbf{p} \in R^{m \times n} \times R^{m \times n} \times R^{m \times n} \times R^{m \times n}$, where div and div^2 respectively denote the adjoint operator of ∇ and ∇^2 , then we have

$$\text{div} \boldsymbol{\rho}_{i,j} = D_x^- \boldsymbol{\rho}_{i,j} + D_y^- \boldsymbol{\rho}_{i,j},$$

$$\text{div}^2 \mathbf{p}_{i,j} = D_x^-(D_x^+ \mathbf{p}_{i,j}) + D_x^-(D_y^+ \mathbf{p}_{i,j}) + D_x^+(D_x^- \mathbf{p}_{i,j}) + D_y^-(D_y^+ \mathbf{p}_{i,j}).$$

In order to discretize (3.8), by using the indicator function (3.10) and the corresponding discrete operators and norms, we can obtain the discretization form as

$$\min_g \|f - \mathcal{A}g\|_2^2 + \lambda(1 - \omega(x)) |\nabla^2 g|_1 + \gamma \omega(x) |\nabla g|_1 + \delta_{\mathcal{D}}(g). \quad (3.12)$$

The problem (3.12) is a nonsmoothing optimization problem. Variable splitting methods such as the alternating direction method of multipliers (ADMM) [42, 15, 43] and the operator splitting methods [31, 37] have been recently used in solving this class of problems. The key of this class of methods is to transform the original problem into some subproblems so that we can easily solve these subproblems by some traditionally numerical methods. By introducing some auxiliary variables $\mathbf{q} = \nabla^2 g$, $\mathbf{v} = \nabla g$ and $z = g$, we convert the problem (3.12) into the following form

$$\begin{cases} \min_{g, \mathbf{q}, \mathbf{v}, z} \|f - \mathcal{A}g\|_2^2 + \lambda(1 - \omega(x))|\mathbf{q}|_1 + \gamma\omega(x)|\mathbf{v}|_1 + \delta_{\mathcal{D}}(z), \\ \text{s.t.} \begin{cases} \mathbf{q} = \nabla^2 g, \\ \mathbf{v} = \nabla g, \\ z = g. \end{cases} \end{cases} \quad (3.13)$$

Then the problem (3.13) can be solved under the framework of the alternating split Bregman method as

$$\begin{cases} (g^{k+1}, \mathbf{q}^{k+1}, \mathbf{v}^{k+1}, z^{k+1}) := \underset{g, \mathbf{q}, \mathbf{v}, z}{\operatorname{argmin}} \|f - \mathcal{A}g\|_2^2 + \lambda(1 - \omega(x))|\mathbf{q}|_1 + \gamma\omega(x)|\mathbf{v}|_1 \\ + \delta_{\mathcal{D}}(z) + \frac{\mu_1}{2} \|\mathbf{b}^k + \nabla^2 g - \mathbf{q}\|_2^2 + \frac{\mu_2}{2} \|\mathbf{c}^k + \nabla g - \mathbf{v}\|_2^2 + \frac{\mu_3}{2} \|d^k + g - z\|_2^2, & (3.14a) \\ \mathbf{b}^{k+1} := \mathbf{b}^k + \nabla^2 g^{k+1} - \mathbf{q}^{k+1}, & (3.14b) \\ \mathbf{c}^{k+1} := \mathbf{c}^k + \nabla g^{k+1} - \mathbf{v}^{k+1}, & (3.14c) \\ d^{k+1} := d^k + g^{k+1} - z^{k+1}. & (3.14d) \end{cases}$$

The minimization problem (3.14a) yielding $(g^{k+1}, \mathbf{q}^{k+1}, \mathbf{v}^{k+1}, z^{k+1})$ is not trivial since it includes two nonseparable terms and two nonsmooth terms. A natural approach is to alternate between minimizing with respect to $g, \mathbf{q}, \mathbf{v}, z$ while keeping others fixed. Then we have the following strategy to solve the problem (3.12)

$$\begin{cases} g^{k+1} := \underset{g}{\operatorname{argmin}} \|f - \mathcal{A}g\|_2^2 + \frac{\mu_1}{2} \|\mathbf{b}^k + \nabla^2 g - \mathbf{q}^k\|_2^2 \\ + \frac{\mu_2}{2} \|\mathbf{c}^k + \nabla g - \mathbf{v}^k\|_2^2 + \frac{\mu_3}{2} \|d^k + g - z^k\|_2^2, & (3.15a) \\ \mathbf{q}^{k+1} := \underset{\mathbf{q}}{\operatorname{argmin}} \lambda(1 - \omega(x))|\mathbf{q}|_1 + \frac{\mu_1}{2} \|\mathbf{b}^k + \nabla^2 g^{k+1} - \mathbf{q}\|_2^2, & (3.15b) \\ \mathbf{v}^{k+1} := \underset{\mathbf{v}}{\operatorname{argmin}} \gamma\omega(x)|\mathbf{v}|_1 + \frac{\mu_2}{2} \|\mathbf{c}^k + \nabla g^{k+1} - \mathbf{v}\|_2^2, & (3.15c) \\ z^{k+1} := \underset{z}{\operatorname{argmin}} \delta_{\mathcal{D}}(z) + \frac{\mu_3}{2} \|d^k + g^{k+1} - z\|_2^2, & (3.15d) \\ \mathbf{b}^{k+1} := \mathbf{b}^k + \nabla^2 g^{k+1} - \mathbf{q}^{k+1}, & (3.15e) \\ \mathbf{c}^{k+1} := \mathbf{c}^k + \nabla g^{k+1} - \mathbf{v}^{k+1}, & (3.15f) \\ d^{k+1} := d^k + g^{k+1} - z^{k+1}. & (3.15g) \end{cases}$$

For the iteration scheme (3.15), we can derive the following convergence result. Though the proof is similar to the course used in [9] and there includes three constrained conditions in solved problem (3.14), the data fitting term in problem (3.13) can make the proof more simple.

Theorem 3.2. *Assume that $\operatorname{Ker}(\mathcal{A}) = \{0\}$ and the point $(g^*, \mathbf{q}^*, \mathbf{v}^*, z^*)$ is the solution of the problem (3.14). Then the sequence $(g^k, \mathbf{q}^k, \mathbf{v}^k, z^k)$ generated by the scheme (3.15) converges to the solution of the problem (3.13) for every choosing original point $(g^0, \mathbf{q}^0, \mathbf{v}^0, z^0)$.*

Proof. The sequence $(g^{k+1}, \mathbf{q}^{k+1}, \mathbf{v}^{k+1}, z^{k+1}, \mathbf{b}^{k+1}, \mathbf{c}^{k+1}, d^{k+1})$ generated by the subproblems (3.15a)-(3.15g) satisfies the following the first order optimization condition as

$$\begin{cases} 0 = \mathcal{A}^*(\mathcal{A}g^{k+1} - f) + \mu_1 \operatorname{div}^2(\nabla^2 g^{k+1} + \mathbf{b}^k - \mathbf{q}^k) \\ \quad \quad \quad - \mu_2 \operatorname{div}(\nabla g^{k+1} + \mathbf{c}^k - \mathbf{v}^k) + \mu_3(g^{k+1} + d^k - z^k), & (3.16a) \\ 0 = \lambda(1 - \omega(x))\mathbf{r}^{k+1} + \mu_1(\mathbf{q}^{k+1} - \mathbf{b}^k - \nabla^2 g^{k+1}), & (3.16b) \\ 0 = \gamma\omega(x)\mathbf{s}^{k+1} + \mu_2(\mathbf{v}^{k+1} - \mathbf{c}^{k+1} - \nabla g^{k+1}), & (3.16c) \\ 0 = \varpi^{k+1} + \mu_3(z^{k+1} - d^k - g^{k+1}), & (3.16d) \\ \mathbf{b}^{k+1} = \mathbf{b}^k + \nabla^2 g^{k+1} - \mathbf{q}^{k+1}, & (3.16e) \\ \mathbf{c}^{k+1} = \mathbf{c}^k + \nabla g^{k+1} - \mathbf{v}^{k+1}, & (3.16f) \\ d^{k+1} = d^k + g^{k+1} - z^{k+1}, & (3.16g) \end{cases}$$

where \mathcal{A}^* , div^2 and div denote the adjoint operator of operators \mathcal{A} , ∇^2 and ∇ , $\mathbf{r}^{k+1} \in \partial(|\mathbf{q}^{k+1}|)$, $\mathbf{s}^{k+1} \in \partial(|\mathbf{v}^{k+1}|)$ and $\varpi^{k+1} \in \partial(\delta_{\mathcal{D}}(z^{k+1}))$. Here $\partial\mathcal{F}(x)$ denotes the subdifferential set at x . By the assumption that the point (g^*, q^*, v^*, z^*) is the solution of the problem (3.14), we can obtain

$$\begin{cases} 0 = \mathcal{A}^*(\mathcal{A}g^* - f) + \mu_1 \operatorname{div}^2(\nabla^2 g^* + \mathbf{b}^* - \mathbf{q}^*) \\ \quad \quad \quad - \mu_2 \operatorname{div}(\nabla g^* + \mathbf{c}^* - \mathbf{v}^*) + \mu_3(g^* + d^* - z^*), & (3.17a) \\ 0 = \lambda(1 - \omega(x))\mathbf{r}^* + \mu_1(\mathbf{q}^* - \mathbf{b}^* - \nabla^2 g^*), & (3.17b) \\ 0 = \gamma\omega(x)\mathbf{s}^* + \mu_2(\mathbf{v}^* - \mathbf{c}^* - \nabla g^*), & (3.17c) \\ 0 = \varpi^* + \mu_3(z^* - d^k - g^*), & (3.17d) \\ \mathbf{b}^* = \mathbf{b}^* + \nabla^2 g^* - \mathbf{q}^*, & (3.17e) \\ \mathbf{c}^* = \mathbf{c}^* + \nabla g^* - \mathbf{v}^*, & (3.17f) \\ d^* = d^* + g^* - z^*, & (3.17g) \end{cases}$$

where $\mathbf{r}^* \in \partial(|\mathbf{q}^*|)$, $\mathbf{s}^* \in \partial(|\mathbf{v}^*|)$ and $\varpi^* \in \partial(\delta_{\mathcal{D}}(z^*))$. Set $g_e^k = g^k - g^*$, $\mathbf{q}_e^k = \mathbf{q}^k - \mathbf{q}^*$, $\mathbf{v}_e^k = \mathbf{v}^k - \mathbf{v}^*$, $\mathbf{r}_e^k = \mathbf{r}^k - \mathbf{r}^*$, $\mathbf{s}_e^k = \mathbf{s}^k - \mathbf{s}^*$, $\varpi_e^k = \varpi^k - \varpi^*$, $\mathbf{b}_e^k = \mathbf{b}^k - \mathbf{b}^*$, $\mathbf{c}_e^k = \mathbf{c}^k - \mathbf{c}^*$, $d_e^k = d^k - d^*$, subtracting (3.17) from (3.16) and then respectively take the inter product $\langle \cdot, \cdot \rangle$ of the left- and right-hand sides by g_e^{k+1} , \mathbf{q}_e^{k+1} , \mathbf{v}_e^{k+1} , z_e^{k+1} , \mathbf{b}_e^k , \mathbf{c}_e^k , d_e^k , we can obtain that

$$\begin{cases} 0 = \|\mathcal{A}g_e^{k+1}\|_2^2 + \mu_1 \|\nabla^2 g_e^{k+1}\|_2^2 + \mu_1 \langle \mathbf{b}_e^k - \mathbf{q}_e^k, \nabla^2 g_e^{k+1} \rangle + \mu_2 \|\nabla g_e^{k+1}\|_2^2 \\ \quad \quad \quad + \mu_2 \langle \mathbf{c}_e^k - \mathbf{v}_e^k, \nabla g_e^{k+1} \rangle + \mu_3 \|g_e^{k+1}\|_2^2 + \mu_3 \langle d_e^k - z_e^k, g_e^{k+1} \rangle, & (3.18a) \\ 0 = \lambda \langle (1 - \omega(x))\mathbf{r}_e^{k+1}, \mathbf{q}_e^{k+1} \rangle + \mu_1 \|\mathbf{q}_e^{k+1}\|_2^2 - \mu_1 \langle \mathbf{b}_e^k + \nabla^2 g_e^{k+1}, \mathbf{q}_e^{k+1} \rangle, & (3.18b) \\ 0 = \gamma \langle \omega(x)\mathbf{s}_e^{k+1}, \mathbf{v}_e^{k+1} \rangle + \mu_2 \|\mathbf{v}_e^{k+1}\|_2^2 - \mu_2 \langle \mathbf{c}_e^k + \nabla g_e^{k+1}, \mathbf{v}_e^{k+1} \rangle, & (3.18c) \\ 0 = \langle \varpi_e^{k+1}, z_e^{k+1} \rangle + \mu_3 \|z_e^{k+1}\|_2^2 - \mu_3 \langle d_e^k + g_e^{k+1}, z_e^{k+1} \rangle, & (3.18d) \\ \langle \mathbf{b}_e^{k+1}, \mathbf{b}_e^k \rangle = \|\mathbf{b}_e^k\|_2^2 + \langle \nabla^2 g_e^{k+1} - \mathbf{q}_e^{k+1}, \mathbf{b}_e^k \rangle, & (3.18e) \\ \langle \mathbf{c}_e^{k+1}, \mathbf{c}_e^k \rangle = \|\mathbf{c}_e^k\|_2^2 + \langle \nabla g_e^{k+1} - \mathbf{v}_e^{k+1}, \mathbf{c}_e^k \rangle, & (3.18f) \\ \langle d_e^{k+1}, d_e^k \rangle = \|d_e^k\|_2^2 + \langle g_e^{k+1} - z_e^{k+1}, d_e^k \rangle. & (3.18g) \end{cases}$$

Since (3.18e)-(3.18g) can be written as

$$\begin{cases} \frac{\mu_1}{2} (\|\mathbf{b}_e^k\|_2^2 - \|\mathbf{b}_e^{k+1}\|_2^2) = \mu_1 \langle \mathbf{b}_e^k, \mathbf{q}_e^{k+1} - \nabla^2 g_e^{k+1} \rangle - \frac{\mu_1}{2} \|\nabla^2 g_e^{k+1} - \mathbf{q}_e^{k+1}\|_2^2 & (3.19a) \\ \frac{\mu_2}{2} (\|\mathbf{c}_e^k\|_2^2 - \|\mathbf{c}_e^{k+1}\|_2^2) = \mu_2 \langle \mathbf{c}_e^k, \mathbf{v}_e^{k+1} - \nabla g_e^{k+1} \rangle - \frac{\mu_2}{2} \|\nabla g_e^{k+1} - \mathbf{v}_e^{k+1}\|_2^2 & (3.19b) \\ \frac{\mu_3}{2} (\|d_e^k\|_2^2 - \|d_e^{k+1}\|_2^2) = \mu_3 \langle d_e^k, z_e^{k+1} - g_e^{k+1} \rangle - \frac{\mu_3}{2} \|g_e^{k+1} - z_e^{k+1}\|_2^2 & (3.19c) \end{cases}$$

Summing (3.18a)-(3.18d) with (3.19a)-(3.19c), we can obtain

$$\begin{aligned}
& \frac{\mu_1}{2}(\|\mathbf{b}_e^k\|_2^2 - \|\mathbf{b}_e^{k+1}\|_2^2) + \frac{\mu_2}{2}(\|\mathbf{c}_e^k\|_2^2 - \|\mathbf{c}_e^{k+1}\|_2^2) + \frac{\mu_3}{2}(\|d_e^k\|_2^2 - \|d_e^{k+1}\|_2^2) \\
&= \|\mathcal{A}g_e^{k+1}\|_2^2 + \mu_1\|\nabla^2 g_e^{k+1}\|_2^2 + \mu_2\|\nabla g_e^{k+1}\|_2^2 + \mu_3\|g_e^{k+1}\|_2^2 + \mu_1\|\mathbf{q}_e^{k+1}\|_2^2 \\
&+ \mu_2\|\mathbf{v}_e^{k+1}\|_2^2 + \mu_3\|z_e^{k+1}\|_2^2 + \lambda\langle(1-\omega(x))\mathbf{r}_e^{k+1}, \mathbf{q}_e^{k+1}\rangle + \gamma\langle\omega(x)\mathbf{s}_e^{k+1}, \mathbf{v}_e^{k+1}\rangle \\
&+ \langle\varpi_e^{k+1}, z_e^{k+1}\rangle - \mu_1\langle\nabla^2 g_e^{k+1}, \mathbf{q}_e^k + \mathbf{q}_e^{k+1}\rangle - \mu_2\langle\nabla g_e^{k+1}, \mathbf{v}_e^k + \mathbf{v}_e^{k+1}\rangle \\
&- \mu_3\langle g_e^{k+1}, z_e^k + z_e^{k+1}\rangle - \frac{\mu_1}{2}\|\nabla^2 g_e^{k+1} - \mathbf{q}_e^{k+1}\|_2^2 - \frac{\mu_2}{2}\|\nabla g_e^{k+1} - \mathbf{v}_e^{k+1}\|_2^2 \\
&- \frac{\mu_3}{2}\|g_e^{k+1} - z_e^{k+1}\|_2^2.
\end{aligned}$$

By summing the above equation from $k = 0$ to $k = \mathcal{K}$, we get

$$\begin{aligned}
& \frac{\mu_1}{2}(\|\mathbf{b}_e^0\|_2^2 - \|\mathbf{b}_e^{\mathcal{K}+1}\|_2^2) + \frac{\mu_2}{2}(\|\mathbf{c}_e^0\|_2^2 - \|\mathbf{c}_e^{\mathcal{K}+1}\|_2^2) + \frac{\mu_3}{2}(\|d_e^0\|_2^2 - \|d_e^{\mathcal{K}+1}\|_2^2) \\
&= \sum_{k=0}^{\mathcal{K}} \left[\|\mathcal{A}g_e^{k+1}\|_2^2 + \lambda\langle(1-\omega(x))\mathbf{r}_e^{k+1}, \mathbf{q}_e^{k+1}\rangle + \gamma\langle\omega(x)\mathbf{s}_e^{k+1}, \mathbf{v}_e^{k+1}\rangle \right. \\
&+ \langle\varpi_e^{k+1}, z_e^{k+1}\rangle + \frac{\mu_1}{2}\|\nabla^2 g_e^{k+1} - \mathbf{q}_e^{k+1}\|_2^2 + \frac{\mu_2}{2}\|\nabla g_e^{k+1} - \mathbf{v}_e^{k+1}\|_2^2 \\
&+ \left. \frac{\mu_3}{2}\|g_e^{k+1} - z_e^{k+1}\|_2^2 \right] + \frac{\mu_1}{2}\|\mathbf{q}_e^{\mathcal{K}+1}\|_2^2 - \frac{\mu_1}{2}\|\mathbf{q}_e^0\|_2^2 + \frac{\mu_2}{2}\|\mathbf{v}_e^{\mathcal{K}+1}\|_2^2 \\
&- \frac{\mu_2}{2}\|\mathbf{v}_e^0\|_2^2 + \frac{\mu_3}{2}\|z_e^{\mathcal{K}+1}\|_2^2 - \frac{\mu_3}{2}\|z_e^0\|_2^2.
\end{aligned}$$

Using the fact that the monotonicity of the subdifferential

$$\begin{cases} \zeta_x \in \partial f(x) \iff f(y) - f(x) \geq \langle \zeta_x, y - x \rangle, & x \in R^n \text{ for } \forall y \in R^n, \\ \zeta_y \in \partial f(y) \iff f(x) - f(y) \geq \langle \zeta_y, x - y \rangle, & x \in R^n \text{ for } \forall y \in R^n, \end{cases}$$

implies

$$\langle \zeta_x - \zeta_y, x - y \rangle \geq 0,$$

we get

$$\begin{aligned}
& \frac{\mu_1}{2}\|\mathbf{b}_e^0\|_2^2 + \frac{\mu_2}{2}\|\mathbf{c}_e^0\|_2^2 + \frac{\mu_3}{2}\|d_e^0\|_2^2 + \frac{\mu_1}{2}\|\mathbf{q}_e^0\|_2^2 + \frac{\mu_2}{2}\|\mathbf{v}_e^0\|_2^2 + \frac{\mu_3}{2}\|z_e^0\|_2^2 \\
&\geq \sum_{k=0}^{\mathcal{K}} \left[\|\mathcal{A}g_e^{k+1}\|_2^2 + \frac{\mu_1}{2}\|\nabla^2 g_e^{k+1} - \mathbf{q}_e^{k+1}\|_2^2 + \frac{\mu_2}{2}\|\nabla g_e^{k+1} - \mathbf{v}_e^{k+1}\|_2^2 \right. \\
&+ \left. \frac{\mu_3}{2}\|g_e^{k+1} - z_e^{k+1}\|_2^2 \right].
\end{aligned}$$

This leads to the following conclusions:

$$\begin{cases} \lim_{k \rightarrow \infty} \|\mathcal{A}g_e^k\|_2^2 = 0, & (3.20a) \end{cases}$$

$$\begin{cases} \lim_{k \rightarrow \infty} \frac{\mu_1}{2}\|\nabla^2 g_e^k - \mathbf{q}_e^k\|_2^2 = 0, & (3.20b) \end{cases}$$

$$\begin{cases} \lim_{k \rightarrow \infty} \frac{\mu_2}{2}\|\nabla g_e^k - \mathbf{v}_e^k\|_2^2 = 0, & (3.20c) \end{cases}$$

$$\begin{cases} \lim_{k \rightarrow \infty} \frac{\mu_3}{2}\|g_e^k - z_e^k\|_2^2 = 0. & (3.20d) \end{cases}$$

By the assumption of $\text{Ker}(\mathcal{A}) = \{0\}$, the formula (3.20a) implies $\lim_{k \rightarrow \infty} g^k = g^*$. Then we also orderly obtain $\lim_{k \rightarrow \infty} \mathbf{q}^k = \mathbf{q}^*$, $\lim_{k \rightarrow \infty} \mathbf{v}^k = \mathbf{v}^*$, $\lim_{k \rightarrow \infty} z^k = z^*$. \square

Remark 3.1. Since we used the periodic boundary condition for the differential operators ∇ and ∇^2 , it is easy to deduce that they are injective operators. So the assumption $\text{Ker}(\mathcal{A}) = \{0\}$ in Theorem 3.2 implies that $\text{Ker}(\mathcal{A}) = \{0\} \cap \text{Ker}(\nabla) \cap \text{Ker}(\nabla^2) = 0$. Then the objective function in the problem (3.12) is strong convexity, therefore the solution is unique. Furthermore, it also means that non-zeros constant images are not included in the null space of the operator \mathcal{A} , which is true for the image deconvolution problem in our numerical implementations.

Remark 3.2. For the dual variables $(\mathbf{b}^k, \mathbf{c}^k, d^k)$ in the iteration schemes (3.15a)-(3.15g), following from the assertions of $(\mathbf{q}^k, \mathbf{v}^k, z^k) \rightarrow (\mathbf{q}^*, \mathbf{v}^*, z^*)$ as $k \rightarrow \infty$ in Theorem 3.2 and equations (3.20b)-(3.20d), we obtain that $\nabla^2 g^* = \mathbf{q}^*$, $\nabla g^* = \mathbf{v}^*$ and $g^* = z^*$. Then we can obtain $(\mathbf{b}^k, \mathbf{c}^k, d^k) \rightarrow (\mathbf{b}^*, \mathbf{c}^*, d^*)$ by taking $k \rightarrow \infty$ in the side of equations (3.15e)-(3.15g) or (3.16e)-(3.16g).

We now consider to solve the subproblem in the scheme (3.15).

- **To solve the subproblem (3.15a):**

The subproblem (3.15a) is a smooth and convex optimization problem, so its Euler-Lagrange equation satisfies

$$\begin{aligned} [\mathcal{A}^* \mathcal{A} + \mu_1 \text{div}^2 \nabla^2 - \mu_2 \text{div} \nabla + \mu_3 I] g^{k+1} &= \mathcal{A}^* f - \mu_1 \text{div}^2 (\mathbf{b}^k - \mathbf{q}^k) \\ &\quad + \mu_2 \text{div} (\mathbf{c}^k - \mathbf{v}^k) - \mu_3 (d^k - z^k), \end{aligned}$$

where \mathcal{A}^* is the conjugate operator of \mathcal{A} . For this equation, we can obtain the explicit solution by using the fast Fourier transform (FFT) while \mathcal{A} has a special form such as the identity operator I or the blurring operator:

$$g^{k+1} = \mathcal{F}^{-1} \left(\frac{M}{D} \right), \quad (3.21)$$

where $M := \mathcal{F}(\mathcal{A}^*) \mathcal{F}(f) - \mu_1 \mathcal{F}(\text{div}^2) \mathcal{F}(\mathbf{b}^k - \mathbf{q}^k) + \mu_2 \mathcal{F}(\text{div}) \mathcal{F}(\mathbf{c}^k - \mathbf{v}^k) - \mu_3 \mathcal{F}(d^k - z^k)$ and $D := \mathcal{F}(\mathcal{A}^* \mathcal{A}) + \mu_1 \mathcal{F}(\text{div}^2 \cdot \nabla^2) - \mu_2 \mathcal{F}(\text{div} \cdot \nabla) + \mu_3 \mathcal{F}(I)$. Here \mathcal{F} denotes the fast Fourier transform and \mathcal{F}^{-1} denotes the inverse of the fast Fourier transform.

- **To solve the subproblem (3.15b) and (3.15c):** The subproblems (3.15b) and (3.15c) have the closed form solution. Since the closed form solution of minimization problem

$$\min_{\varrho} \frac{\xi}{2} \|\varrho - \varpi\|_2^2 + |\varrho|_1$$

is

$$\varrho = \max \left\{ |\varpi|_1 - \frac{1}{\xi}, 0 \right\} \frac{\varpi}{|\varpi|_1}$$

for $\varrho, \varpi \in R^s$ and $\xi > 0$, then the solution of the problems (3.15b) and (3.15c) can be denoted as

$$\left\{ \mathbf{q}^{k+1} = \max \left\{ |\bar{h}|_1 - \frac{\lambda(1 - \omega(x))}{\mu_1}, 0 \right\} \frac{\bar{h}}{|\bar{h}|_1} \right. \quad (3.22a)$$

$$\left. \mathbf{v}^{k+1} = \max \left\{ |\mathfrak{S}|_1 - \frac{\gamma \omega(x)}{\mu_2}, 0 \right\} \frac{\mathfrak{S}}{|\mathfrak{S}|_1}, \right. \quad (3.22b)$$

where $\bar{h} = \mathbf{b}^k + \nabla^2 g^{k+1}$ and $\mathfrak{S} = \mathbf{c}^k + \nabla g^{k+1}$.

- **To solve the subproblem (3.15d):** The subproblem is the projection problem on the convex set \mathcal{D} . So its solution can be obtained by

$$z^{k+1} := \max \left\{ \min \{ d^k + g^{k+1}, \iota \}, 0 \right\}. \quad (3.23)$$

3.3 The K-means clustering threshold

With the development and improvement of data mining technology, data clustering algorithm is gradually applied to some fields. Among clustering algorithms, the K -means clustering method can be applied in many fields which include image and audio data compression, preprocess of system modeling with radial basis function networks, and task decomposition of heterogeneous neural network structure.

The clustering method of K -means originally proposed in [30] is a data mining algorithm which performs clustering by using an iterative approach. It takes the number or desired clusters and the initial means as input and produces final means as output. If the algorithm is required to produce K clusters, then there will be K initial means and K final means. After termination of the K -means clustering, each object in dataset becomes a member of one cluster. It can provide relatively good result for convex cluster with relatively flexible and high efficient. Though this method is sensitive to the choice of starting points and can only be applied to a small dataset, in our experiment we still obtain suitable segmentation results. So we use it to obtain some suitable thresholds for the image segmentation problem. In order to segment the restored image g generated by the first step, we first linearly stretched it \bar{g} in the second step by the strategy as

$$\bar{g} = \frac{g - g_{\min}}{g_{\max} - g_{\min}},$$

where g_{\min} and g_{\max} represent minimum and maximum of g respectively. Denote $\rho_1 \leq \rho_2 \leq \dots \leq \rho_K$ to be the centers of the K clusters use K as follows $K - 1$ of the pixel intensities of the restored image. Here we define the $K - 1$ thresholds to be $\bar{\rho}_i = (\rho_i + \rho_{i+1})/2$. Denote $\rho_0 = 0$ and $\rho_K = 1$, then the i -th phase of \bar{g} is given by $\{x : \bar{\rho}_{i-1} \leq \bar{g} \leq \bar{\rho}_i\}$.

4 Numerical implementation and experimental results

In this section, we arrange some experimental comparisons from our proposed method with other recent methods [8, 18, 27, 44, 45]. Following from the primal-dual approach, the authors in [8] extended the method developed in [1] to solve the continuous Potts model with applications to the multiphase piecewise constant Mumford-Shah model, where the numerical comparisons illustrated that their method outperforms some methods reviewed in [1]. On the other hand, the method in [1] has exhibited the strength over those popular methods such as the α expansion and α - β swap [7], the method of Pock et al. [11], and the algorithm in Lellmann et al. [22]. For the strategy in [18], its numerical results showed that they outperform the methods used in [1, 11, 24]. In experiments, the model (2.6) is different to other models since we first need to know mean values in every segmentation region. To summarize, the two-stage image segmentation scheme is written as follows:

Algorithm 4.1. *Solving the two-stage image segmentation model (3.8) with the clustering method:*

- **Step 1.** Choose original values $g^0 = f$, $\mathbf{b}^0 = \mathbf{q}^0 = \mathbf{0}$, $\mathbf{c}^0 = \mathbf{v}^0 = \mathbf{0}$, $d^0 = 0$. Set $k = 0$;
- **Step 2.** Compute values of $(g^k, \mathbf{q}^k, \mathbf{v}^k, \mathbf{b}^k, \mathbf{c}^k, d^k)$ by the strategies (3.21)-(3.23). If the stopping criterion is satisfied, output g and do the next step;
- **Step 3.** Apply K -means method to obtain the cluster and then get the mean value of each cluster $\rho_1 \leq \rho_2 \leq \dots \leq \rho_K$. Set the thresholds as $\bar{\rho}_i = (\rho_i + \rho_{i+1})/2$ and then get the segmentation image.

In the numerical implementation, all of parameters are chosen optimally with respect to the chosen dataset by trials and errors by getting the best segmentation results. The stopping criterion is of reaching the maximum iteration number \mathcal{K} or of satisfying $\min \left\{ \|\mathbf{b}^{k+1} - \mathbf{b}^k\|_2, \|\mathbf{c}^{k+1} - \mathbf{c}^k\|_2, \|d^{k+1} - d^k\|_2 \right\} \leq \epsilon$, where ϵ denotes a small positive number defined by the user. It is worth noting that it is suitable for running the inner loop of the proposed algorithm, we however set it to be one and find that we also get the pleasing numerical results. For the original image, we normalize it into the range $[0, 1]$, so we need to set $\iota = 1$ for the constraint in our proposed model. For the weighed function $w(x)$, it can weaken the influence of noise as the form $\omega(x) = \frac{1}{1 + \varsigma \|\nabla f_\sigma\|_2^2}$, where $f_\sigma = G_\sigma * f$. Here G_σ denotes the Gaussian kernel function with the standard deviation σ , $'*$ ' is the convolution operation and ς is a scalar parameter. Furthermore, in order to simplify notations of those previous methods, we set the method used in [14] to solve the CV model (2.2) to be the CVM, the method used the max flow method in [44, 45] to solve the Potts-type model in (2.6) as the MFPM(max flow method for the Potts-type model), the method used the new primal dual method in [18] to solve the Potts-type model in (2.6) as the PDPM(primal dual method for the Potts-type model), the method used the two step in [8] for solving the Mumford-Shah model (2.7) to be the TSMSM(two step for the Mumford-Shah model). Moreover, we set our proposed method by using the Algorithm 4.1 as the HTVWM. Simultaneously, we use the method similar to Algorithm 4.1 to solve the unstrained model (removing the term $g \in [0, \iota]$ in (3.8)) as the HTVUM in order to show the effectiveness of the constrained problem (3.8). As we know that the K-means method is a local method so we run each method ten times and then choose their average value.

For degraded images, we used Matlab functions “**imfilter**” and “**imnoise**” to generate noise and blurring effects. Here we only use blurring kernels of Gaussian and motion. For the convenience of description, we denote the Gaussian blur with a blurring size s and a standard deviation σ_g as (G, s, σ_g) . Similarly, the motion blur with a motion length ι and an angle θ is denoted as (M, ι, θ) . To more fairly tune parameters, we save the corrupted image as the “**mat**” format and then load it in numerical experiments. All the experiments are run with the Matlab code on the work station of CPU 2.4GHz with RAM 4.00G.

4.1 Piecewise constant image segmentation

In this subsection, we use two artificial synthetic piecewise constant images shown in Figure 4.1 as the testing images. The left image includes a simpler geometrical structures with two different intensities, but the right image includes more complicated boundaries with three different

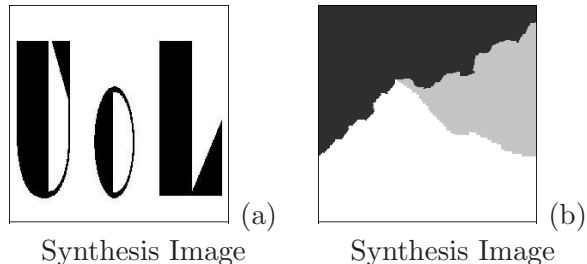


Figure 4.1: The original image used in Example 4.1 and 4.2.

intensities. Since the original segmentation results can be accurately obtained for these images,

we define the segmentation accuracy(SA) as

$$SA = \frac{\text{Number of uncorrectly classified pixels}}{\text{Total number of pixels}} \times 100\%$$

in order to evaluate the accuracy of the used models.

Example 4.1. We choose Figure 4.1(a) for testing and comparison. The degraded images are shown in Figure 4.2. In Figure 4.3-4.5, we show some segmentation results generated by using six

| Methods | Fig. 1 | Fig. 2 | Fig.3 |
|---------|--------------|--------------|--------------|
| CVM | 1.42% | 1.14% | 5.17% |
| MFPM | 0.98% | 1.05% | 2.29% |
| PDPM | 0.85% | 0.84% | 2.06% |
| TSMSM | 0.72% | 0.82% | 1.39% |
| HTVUM | 0.70% | 0.65% | 1.18% |
| HTVWM | 0.72% | 0.60% | 1.16% |

Table 4.1: The SA in Example 4.1.

kinds of aforementioned different models and methods, where the test image "UOL" is segmented into two phases as foreground and background. The related results are arranged in Table 4.1.

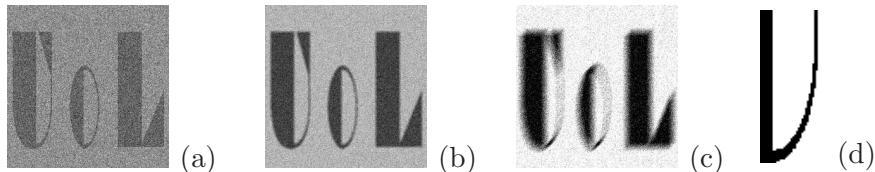


Figure 4.2: Some related images used in Example 4.1. (a). Contaminated by the white Gaussian noise with the variance 0.1; (b). Contaminated by the Gaussian blur ($G, 5, 5$) and the white Gaussian noise with the variance 0.1; (c). Contaminated by the motion blur ($M, 21, 45$) and the white Gaussian noise with the variance 0.01; (d). A part of "U" in "UOL".

As we can see from Figure 4.3, nearly all models exhibit a similar segmentation performance to the noisy image shown in Figure 4.2(a) except for the CVM [14]. This is because of needing to choose the global constant for the CV model. For the blurring images in Figure 4.2(b) and 4.2(c), the CVM [14] and the MFPM and PDPM based on the Potts-type model can not obtained efficient segmentation due to the blurring edge structures. For other three models, the degraded information has been efficiently suppressed before using the K-means method to segmentation, so we can get better segmentation results. Furthermore, our proposed model (3.8) yields the best segmentation results because of adding the constraint and using the hybrid total variation space. We also see from Table 4.1 that our proposed algorithm has a smaller SA values. Related results can be also seen from the magnified portion of the letter U in Figure 4.3-4.5.

Example 4.2. The objective of this example is to illustrate the influence of the contaminated level on the segmentation results. We do not investigate the explicit relationship between all levels and the segmentation accuracy in this work. Instead, we empirically selected three class of contamination to show the influence of segmentation. As we can see from Example 4.1 that the CVM [14], the MFPM [44, 45] and the PDPM [18] can not efficiently segment the degraded image, so we only consider other three segmentation schemes based on the two-step strategy. Table 4.2 demonstrates the chosen parameter γ by fixing the other parameter λ in models and the segmentation accuracy

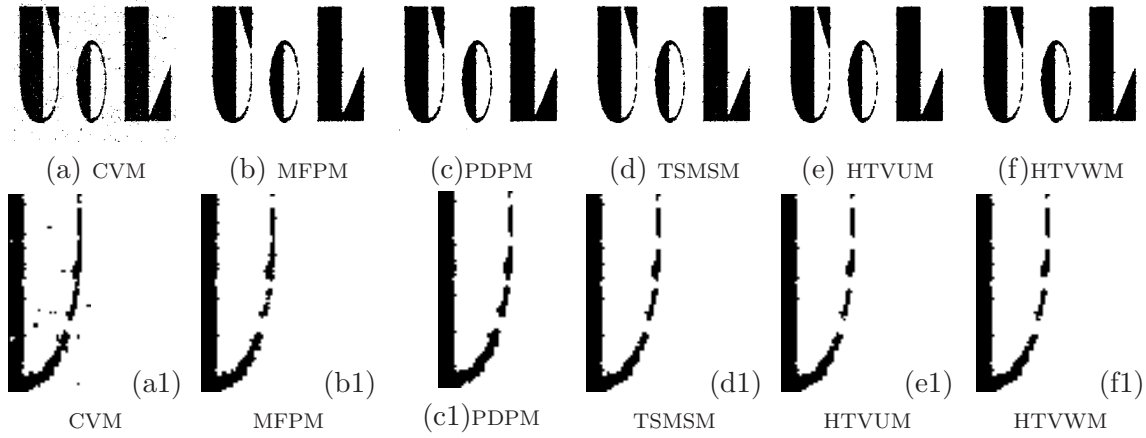


Figure 4.3: Comparison of segmentation results by using differential models for the noisy two-phase image in Example 4.1. (a): The noisy image; (a1): The magnified portion of the original image; Row 2 (b1)-(f1): the magnified portion of the images corresponding to Row 1 (b)-(f). Parameters: (b): $\gamma = 200$; (c): $\gamma = 0.65$; (d): $\gamma = 2.1$ and $\lambda = 0.02$; (e): $\gamma = 1.95$ and $\lambda = 0.2$; (f): $\gamma = 1.95$ and $\lambda = 0.1$.

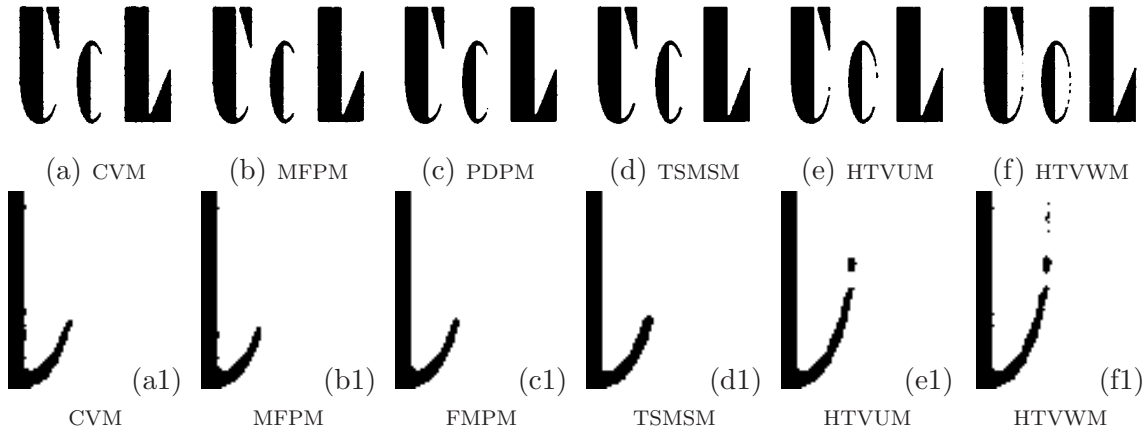


Figure 4.4: Comparison of segmentation results by using differential models for the noisy two-phase image in Example 4.1. (a): The noisy image; (a1): The magnified portion of the original image; Row 2 (b1)-(f1): the magnified portion of the images corresponding to Row 1 (b)-(f). Parameters: (b): $\gamma = 330$; (c): $\gamma = 0.55$; (d): $\gamma = 9.0$ and $\lambda = 0.01$; (e): $\gamma = 11.25$ and $\lambda = 0.03$; (f): $\gamma = 11.75$ and $\lambda = 0.0075$.

(SA) by using Figure 4.1(b) as the testing image. Our proposed constrained model can obviously improve segmentation results upon the HTVUM and the TSMSM especially at high noise levels and blurring effects. Actually, it is due to that the information of edges and constraint in our proposed model can efficiently suppress noise and preserve edges. Simultaneously, we find out that the parameter γ increases with the degraded level. Actually, this is because of that we need to increase the weighted values for penalising the regularization terms in models when the image contamination increases.

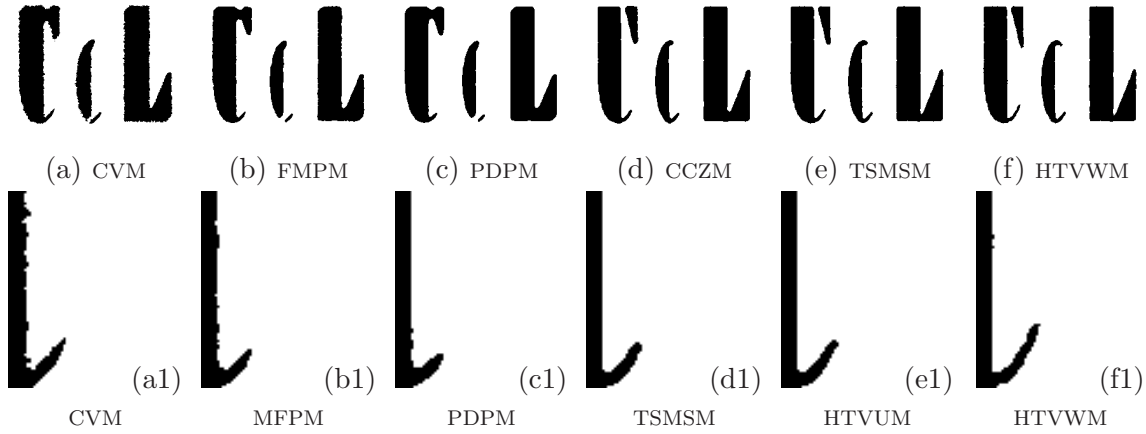


Figure 4.5: Comparison of segmentation results by using differential models for the noisy two-phase image in Example 4.1. (a): The noisy image; (a1): The magnified portion of the original image; Row 2 (b1)-(f1): the magnified portion of the images corresponding to Row 1 (b-)-(f). Parameters: (b): $\gamma = 200$; (c): $\gamma = 0.15$; (d): $\gamma = 11$ and $\lambda = 0.001$; (e): $\gamma = 21.5$ and $\lambda = 0.02$; (f): $\gamma = 26$ and $\lambda = 0.8$.

4.2 Inhomogeneous image segmentation

In this subsection, we extend our proposed method to segment two classes of inhomogeneous images shown in Figure 4.6. The left is a synthesized image by combining the arterial blood vessels of a human head. The right is a MRI brain image based on an anatomical model of normal brain from the slice 91 of the normal brain database, which is available to the public at <http://www.bic.mni.mcgill.ca/brainweb/>. Here we set as “modality=T1, Slice thickness=1mm, intensity non-uniformity = 20%” for the original image 4.6(b). Different to the numerical comparisons of the piecewise constant image, we do not know the real segmentation due to the inhomogeneity. So we except to obtain a better restored image as the stopping condition in the first step of our proposed strategy.

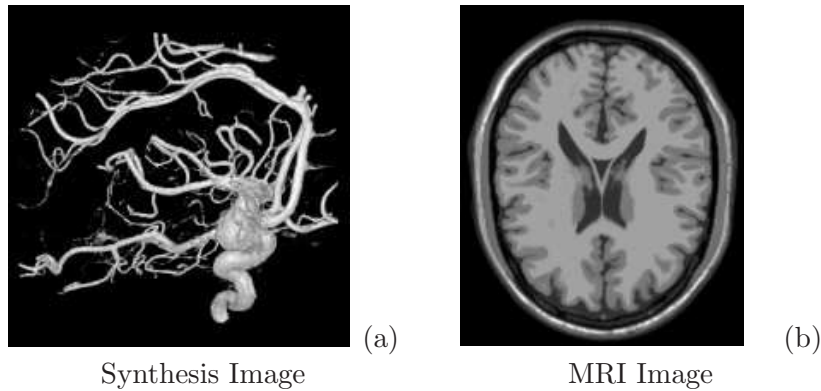


Figure 4.6: The original images in Example 4.3 and 4.4.

Example 4.3. Figure 4.7 presents the applications of our proposed model to segment synthesis degraded images into two phases by using the different methods. It is clear that our proposed method can efficiently segment image, especially in the region of the endings of image. Actually, the proposed method (3.8) can keep the information of edges due to the penalty of the weighted

| Variables | $\sigma = 0.005$ | | $\sigma = 0.01$ | | $\sigma = 0.02$ | |
|-----------|----------------------------|-------------|------------------------------------|-------------|-----------------------------|-------------|
| | γ/λ | SA(%) | γ/λ | SA(%) | γ/λ | SA(%) |
| TSMSM | 18/0.005 | 0.79 | 11/0.005 | 0.13 | 6.0/0.005 | 0.29 |
| HTVUM | 17/0.5 | 0.87 | 9.0/0.5 | 0.14 | 6.2/0.5 | 0.33 |
| HTVWM | 7.0/0.35 | 0.78 | 4.0/0.35 | 0.13 | 2.3/0.35 | 0.29 |
| Variables | $(G, 5, 5)/\sigma = 0.01$ | | $(G, 7, 7)/\sigma = 0.02$ | | $(G, 9, 9)/\sigma = 0.03$ | |
| | γ/λ | SA(%) | γ/λ | SA(%) | γ/λ | SA(%) |
| TSMSM | 13/0.02 | 0.55 | 8.9/0.02 | 0.92 | 4.5/0.02 | 1.30 |
| HTVUM | 41/0.15 | 0.77 | 34/0.15 | 1.29 | 24/0.15 | 1.70 |
| HTVWM | 13/0.6 | 0.54 | 7.0/0.6 | 0.87 | 3.5/0.6 | 1.14 |
| Variables | $(M, 5, 10)/\sigma = 0.01$ | | $(M, 10, 20)/\gamma/\sigma = 0.02$ | | $(M, 15, 30)/\sigma = 0.03$ | |
| | γ/λ | SA(%) | γ/λ | SA(%) | γ/λ | SA(%) |
| TSMSM | 11/0.02 | 0.39 | 5.0/0.02 | 1.0 | 2.8/0.02 | 1.24 |
| HTVUM | 19/0.15 | 0.48 | 19/0.15 | 1.36 | 14/0.15 | 1.76 |
| HTVWM | 12/0.6 | 0.39 | 5.0/0.6 | 0.96 | 3.0/0.6 | 1.14 |

Table 4.2: The related data in Example 4.2.

function $w(x)$. The related parameters and data can be found in the caption of Figure 4.7.

Example 4.4. We consider our proposed method to segment a four-region of the real brain MRI images shown in Figure 4.6, where the regions include the grey matter, the white matter, the tumor-bone, and the background region respectively. The degraded images are shown in Figure 4.8. The first column of Figure 4.9 and 4.10 is the background showing as the white regions in the first column. Due to the little importance of the background, we essentially treat the problem as a 3-phase problem with the black background ordered in the second to fourth column of all our results. The tumor region is ordered in the second column, the grey matter is ordered in the third column, and the white matter is ordered in the fourth column. All the images provide valuable information about the corresponding regions. Obviously, the HTVWM can efficiently segment the tumor region and the white matter region quite well.

5 Conclusions

In this paper, we proposed a two step strategy to segment the contaminated image by combining the hybrid total variation model (3.8) and K-means clustering method. The model (3.8) convexly combined the total variation functional and the high order total variation functional with a weighted balance to obtain efficient restored image. In order to solve this nonsmoothing model, we used the alternating split Bregman method and also analyzed its convergence. Once the restored image is obtained, we clustered it into the expected phase by using the K-means clustering method. Numerical experiments illustrated the effectiveness of our proposed method compared with the methods in [14, 18, 8]. In the experiments we found that a better restoration image did not imply a better segmentation result. So choosing a suitable restoration measure is very important and is also a part of the future work.

Acknowledgments

We would like to thank Dr. Huibin Chang for his suggestions on the numerical experiments and anonymous referees for their helpful comments and suggestions for improving this paper.

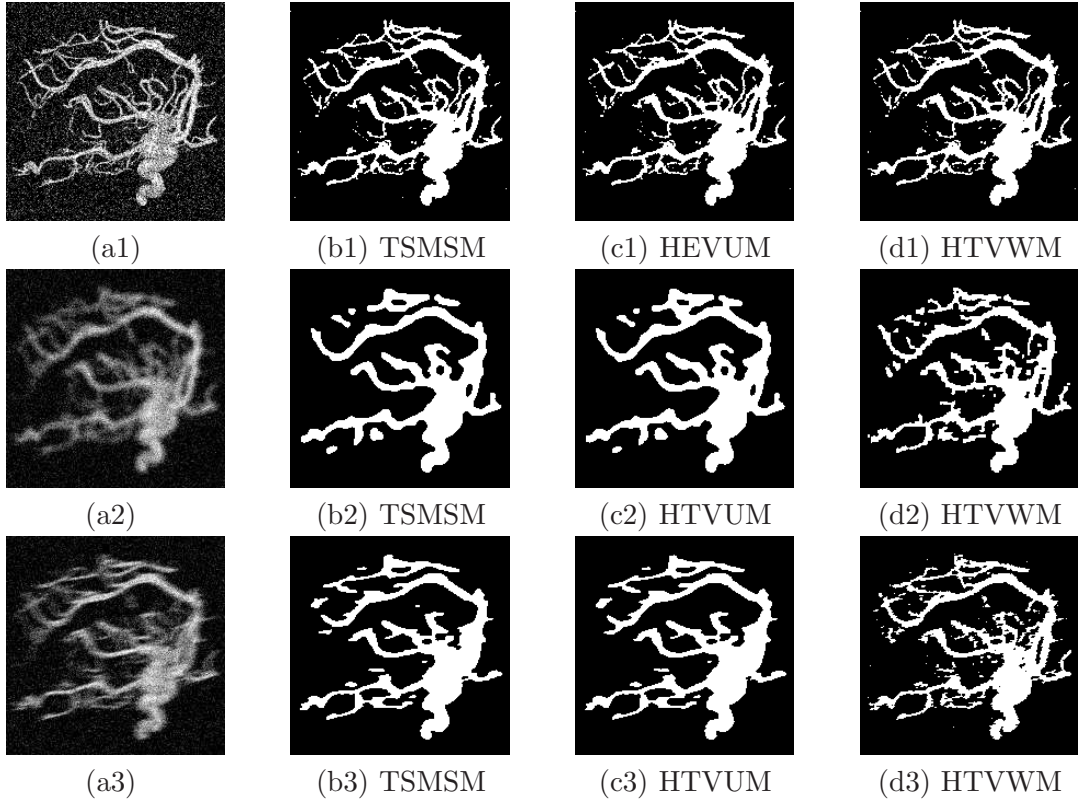


Figure 4.7: Comparison of segmentation results by using different models for the noisy two-phase image. (a1)-(a3) Contaminated images: (a1) $\sigma = 0.05$; (a2) $(G, 7, 7)$ and $\sigma = 0.01$; (a3) $(M, 10, 10)$ and $\sigma = 0.01$. Related parameters in models. (b1) $\gamma = 7.7$ and $\lambda = 0.6$; (c1) $\gamma = 8$ and $\lambda = 0.2$; (d1) $\gamma = 7.6$ and $\lambda = 0.2$; (b2) $\gamma = 20$ and $\lambda = 20$; (c2) $\gamma = 17.3$ and $\lambda = 0.003$; (d2) $\gamma = 161$ and $\lambda = 0.2$; (b3) $\gamma = 24$ and $\lambda = 0.01$; (c3) $\gamma = 20$ and $\lambda = 0.03$; (d3) $\gamma = 147$ and $\lambda = 0.0075$.

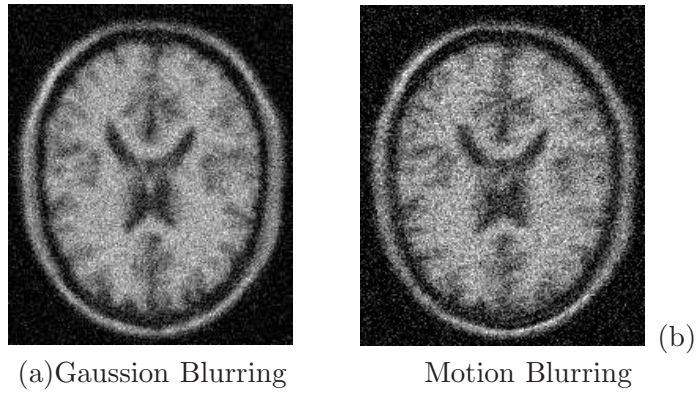


Figure 4.8: The contaminated image in Example 4.4. (a) $(G, 5, 5)$ and $\sigma = 0.01$; (b) $(M, 7, 15)$ and $\sigma = 0.02$.

References

- [1] E. Bae, J. Yuan, and X.-C. Tai, Global minimization for continuous multiphase partitioning problems using a dual approach, *International Journal of Computer Vision*, **92**(1)(2011),

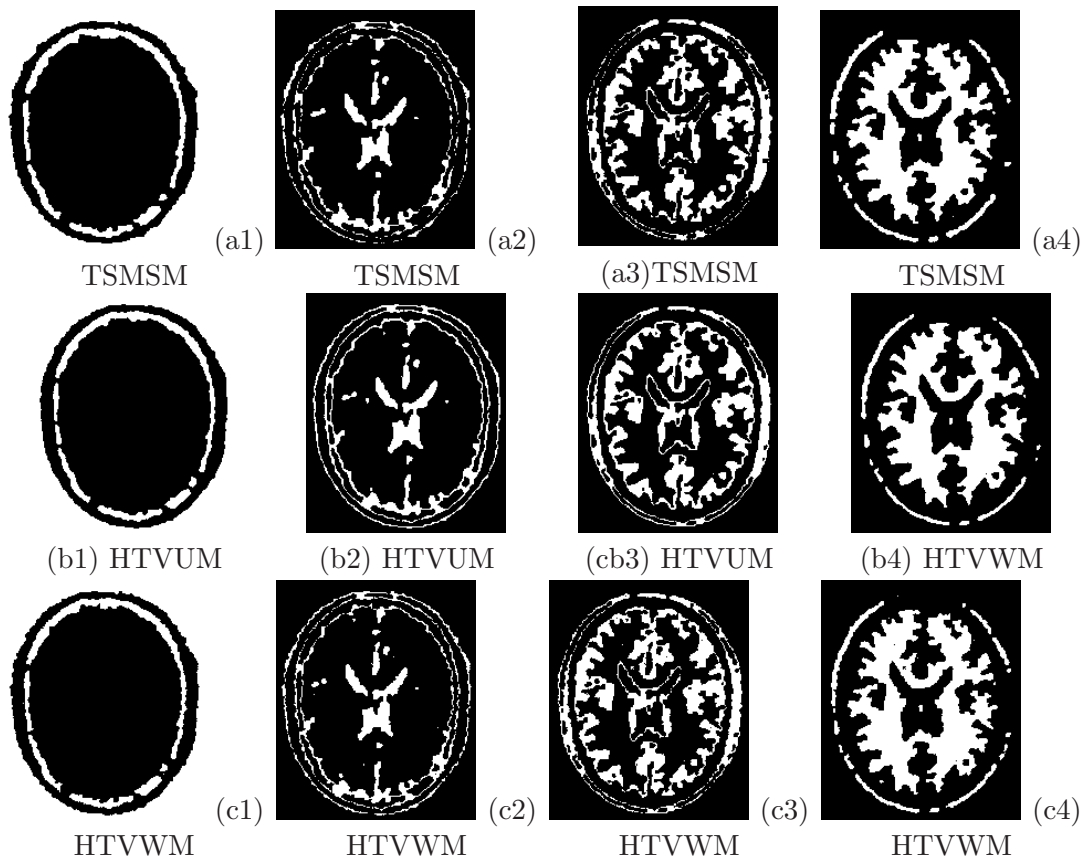


Figure 4.9: Comparisons of the four-phase segmentation results generated by the TSMSM, HTVUM, and HTVWM. Column: First: Background; Second: Tumor and bone; Third: Gray Matter; Forth: White matter. Parameters-TSMSM: $\lambda = 51$ and $\gamma = 0.03$; HTVUM: $\lambda = 44$ and $\gamma = 0.01$; HTVWM: $\lambda = 54$ and $\gamma = 0.008$.

112-129.

- [2] Y. Boykov, O. Veksler, and R. Zabih, Fast approximate energy minimization via graph cuts, *IEEE Transactions on Pattern Analysis and Machine Intelligence*, **23(11)**(2001), 1-18.
- [3] K. Bredies, K. Kunisch, and T. Pock. Total generalized variation. *SIAM Journal on Imaging Sciences*, **3(3)**(2010):492-526.
- [4] X. Bresson, S. Esedoglu, P. Vanderghenst, J. Thiran, and S. Osher, Fast global minimization of the active contour/snake model, *Journal of Mathematical Imaging and Vision*, **28(2)**(2007), 151-167.
- [5] E. S. Brown, T. F. Chan, and X. Bresson, Completely convex formulation of the Chan-Vese image segmentation model, *International Journal of Computer Vision*, **98(1)**(2012), 103-121.
- [6] Y. Boykov, V. Kolmogorov, D. Cremers, and A. Delong, An integral solution to surface evolution PDEs via geo-cuts. *Proc. ECCV LNCS 3953*(2006), 409C422 (2006)
- [7] Y. Boykov, O. Veksler, and R. Zabih, Fast approximate energy minimization via graph cuts, *IEEE Transactions on Pattern Analysis and Machine Intelligence*, **23(11)**(2001), 1222-1239.

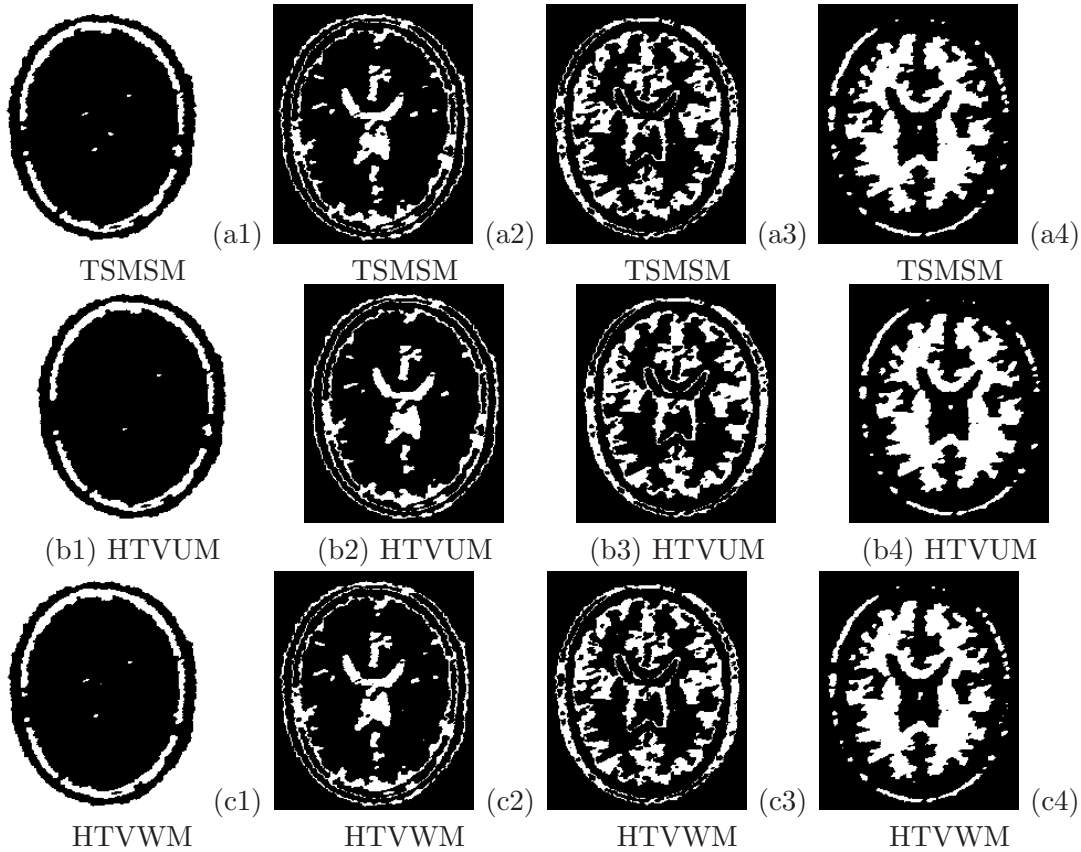


Figure 4.10: Comparisons of the four-phase segmentation results generated by the TSMSM, HTVUM, and HTVWM. Column: First: Background; Second: Tumor and bone; Third: Gray Matter; Forth: White matter. Parameters-TSMSM: $\lambda = 29$ and $\gamma = 0.4$; HTVUM: $\lambda = 25$ and $\gamma = 0.04$; HTVWM: $\lambda = 26$ and $\gamma = 0.02$.

- [8] X. Cai, R. Chan, and T. Zeng, A two-stage image segmentation method using a convex variant of the Mumford-Shah model and thresholding, *SIAM Journal on Image Science*, **6(1)**(2013), 368-390.
- [9] J.-F. Cai, S. Osher, and Z. Shen, Split Bregman methods and frame based image restoration, *SIAM: Multiscale Modeling and Simulation*, **8(2)**(2009), 337-369.
- [10] V. Caselles, R. Kimmel, and G. Sapiro, Geodesic active contours, *International Journal of Computer Vision*, **22(1)**(1997), 61-79.
- [11] A. Chambolle, D. Cremers, and T. Pock, A convex approach to minimal partitions, *SIAM Journal on Image Science*, **5(4)**(2012), 1113-1158.
- [12] T. Chan, S. Esedoglu, and M. Nikolova, Algorithms for finding global minimizers of image segmentation and denoising models, *SIAM Journal on Applied Mathematics*, **66(5)**(2006), 1632-1648.
- [13] T. Chan, A. Marquina, and P. Mulet, High-order total variation-based image restoration, *SIAM Journal on Scientific Computing*, **22(2)**(2000), 503-516.
- [14] T. Chan and L. Vese, Active contours without edges, *IEEE Transactions on Image Processing*, **10(2)**(2001), 266-77.

- [15] C. Chen, B. He, and X. Yuan, Matrix completion via an alternating direction method, *IMA Journal of Numerical Analysis*, **32(1)**(2012), 227-245.
- [16] A. Delong, A. Osokin, H. Isack, and Y. Boykov, Fast approximate energy minimization with label costs, *International Journal of Computer Vision*, **96(1)**(2012), 1-27.
- [17] S. Esedoglu and Y. Tsai, Threshold dynamics for the piecewise constant Mumford-Shah functional, *Journal of Computational Physics*, **211(1)**(2006), 367-384.
- [18] Y. Gu, L.-L. Wang, and X.-C. Tai, A direct approach towards global minimization for multiphase labeling and segmentation problems, *IEEE Transactions on Image Processing*, **21(5)**(2012), 2399-2411.
- [19] L. Grady, The piecewise smooth Mumford-Shah functional on an arbitrary graph. *IEEE Transactions on Image Processing*. textbf18(11)(2009), 2547-2561.
- [20] M. Kass, A. Witkin, and D. Terzopoulos, Snakes: Active contour models, *International Journal of Computer Vision*, **1(4)**(1988)321-331.
- [21] J. Lellmann, B. Lellmann, F. Widmann, and C. Schnorr, Discrete and continuous models for partitioning problems, *International Journal of Computer Vision*, **104(3)**(2013), 241-269.
- [22] J. Lellmann, J. Kappes, J. Yuan, F. Becker, and C. Schnoor, Convex multi-class image labeling by simplex-constrained total variation, *Scale Space and Variational Methods in Computer Vision*, **5567**(2009), 150-162.
- [23] J. Lellmann and C. Schnoor, Continuous multiclass labeling approaches and algorithms, *Journal of Imaging Science*, **4(4)**(2011), 1049-1096.
- [24] F. Li, M. Ng, T. Y. Zeng, and C. Shen, A multiphase image segmentation method based on fuzzy region competition, *SIAM Journal on Scientific Computing*, **3(3)**(2010), 277-299.
- [25] F. Li, C. Shen, J. Fan, and C. Shen, Image restoration combining a total variational filter and a fourth-order filter, *Journal of Visual Communication and Image Representation*, **18(4)**(2007), 322-330.
- [26] J. Lie, M. Lysaker, and X.-C. Tai, A variant of the level set method and applications to image segmentation, *Mathematics of Computation*, **75(255)**(2006), 1155-1174.
- [27] J. Lie, M. Lysaker, and X.-C. Tai, A binary level set model and some applications to Mumford-Shah image segmentation, *IEEE Transactions on Image Processing*, **15(5)**(2006), 1171-1181.
- [28] M. Lysaker, A. Lundervold, and X. Tai, Noise removal using fourth-order partial differential equation with applications to medical magnetic resonance images in space and time, *IEEE Transactions on Image Processing*, **12(12)**(2003), 1579-1590.
- [29] D. Krishnan, Q. Pham, and A. Yip. A primal-dual active-set algorithm for bilaterally constrained total variation deblurring and piecewise constant Mumford-Shah segmentation problems. *Advances in Computational Mathematics*, **31(1-3)**(2009), 237-266.
- [30] B. Macqueen, Some methods for classification and analysis of multivariate observations, *In: Proceedings of 5th Berkeley Symposium on Mathematical Statistics and Probability*, **1**(1967), 281-297.

- [31] A. Marquina and S. J. Osher, Image super-resolution by TV-regularization and Bregman iteration, *Journal of Scientific Computing*, **37(3)**(2008), 367-382.
- [32] D. Mumford and J. Shah, Optimal approximations by piecewise smooth functions and associated variational problems, *Communications on Pure and Applied Mathematics*, **42(5)**(1989), 577-685.
- [33] C. Nieuwenhuis, E. Toppe, and D. Cremers, A survey and comparison of discrete and continuous multi-label optimization approaches for the Potts model, *International Journal of Computer Vision*, **104(3)**(2013), 223-240.
- [34] K. Papafitsoros and C. Schonlieb, A combined first and second variational approach for image reconstruction, *Journal of Mathematical Imaging and Vision*, **48(2)**(2014), 308-338.
- [35] T. Pock, A. Chambolle, H. Bischof, and D. Cremers, A convex relaxation approach for computing minimal partitions, *In: IEEE Conference on Computer Vision and Pattern Recognition(CVPR)*, (2009), 810-817.
- [36] L. Rudin, S. Osher, and E. Fatemi, Nonlinear total variation based noise removal algorithms, *Physica D*, **60(1-4)**(1992), 259-268.
- [37] S. Setzer, Split Bregman algorithm, Douglas-Rachford splitting and frame shrinkage, *In Proceedings of the Second International Conference on Scale Space and Variational Methods in Computer Vision*, **5567**(2009), 464-476.
- [38] R. Schafer, R. Mersereau, and M. Richaards. Constrained iterative restoration algorithms. *Proceedings of the IEEE*, **69(4)**(1981), 432-450.
- [39] O. Tobias and R. Seara, Image segmentation by histogram thresholding using fuzzy sets, *IEEE Transactions on Image Processing*, **11(12)**(2002), 1457-1465.
- [40] L. Vese and T. Chan, A multiphase level set framework for image segmentation using the MumfordCShah model, *International Journal of Computer Vision*, **50(3)**(2002), 271-293.
- [41] X. Wang, D. Huang, and H. Xu, An efficient local Chan-Vese model for image segmentation, *Pattern Recognit*, **43(3)**(2010), 603-618.
- [42] C. Wu and X. Tai, Augmented Lagrangian method, dual methods, and split Bregman iteration for ROF, vectorial TV, and high order models, *SIAM Journal on Imaging Sciences*, **3(3)**(2010), 300-339.
- [43] J. Yang and Y. Zhang, Alternating direction algorithms for ℓ^1 problems in compressive sensing, *SIAM Journal on Scientific Computing*, **33(1)**(2011), 250-278.
- [44] J. Yuan, E. Bae, X.-C. Tai, and Y. Boykov, A continuous max-flow approach to Potts model, *11th European Conference on Computer Vision (ECCV)*, (2010), 379-392.
- [45] J. Yuan, E. Bae, X.-C. Tai, and Y. Boykov, A study on continuous max-flow and min-cut approaches, *IEEE Conference on Computer Vision and Pattern Recognition (CVPR)*, (2010), 2217-2224.
- [46] J. Yuan, C. Schnörr, and Gabriele Steidl, Total-variation based piecewise affine regularization. *Scale Space and Variational Methods in Computer Vision*, **5567**(2009), 552-564.

- [47] C. Zach, D. Gallup, J. Frahm, and M. Niethammer, Fast global labeling for real-time stereo using multiple plane sweeps, *In: Vision, modeling, and visualization*, (2008)243-252.
- [48] R. Zhang, X. Bresson, and X.-C. Tai, Four color theorem and convex relaxation for image segmentation with any number of regions, *Inverse Problems and Imaging*, **7(3)**(2013), 1099-1113.
- [49] S. Zhu and A. Yuille, Region competition: unifying snakes, region growing, and Bayes/MDL for multi-band image segmentation, *IEEE Transactions on Pattern Analysis and Machine Intelligence*, **18(9)**(1996), 884-900.

Received May 2014; revised July 2015, accepted April 2016 by Inverse problem and Imaging.